ARTICLE

Trends of Satellite-Derived Thermal Fronts in the Southeast and Southwest of Australia Between 1993 and 2019

Kai Yang[1,2] · Andrew M. Fischer[1] · Pallavi Govekar[3]

Abstract

Oceanic fronts play a significant role in marine ecosystems by enhancing vertical exchange, promoting the aggregation of plankton, and drawdown of organic carbon. Anthropogenic emission of carbon dioxide and other greenhouse gases in the twentieth century has driven global warming, leading to rising ocean temperatures. Specific regions warming faster than the global average—known as 'ocean warming hotspots'—have been identified, impacting geophysical and biogeochemical dynamics of local ecosystems. Here, we aim to characterize the variability of sea surface temperature (SST) fronts in the southeast and southwest Australia hotspots. Using a histogram frontal detection method, we derived fronts from AVHRR-only and Multi-sensor 6-day SST composites on a 0.02×0.02 grid between January 1993 and December 2019. Our results indicate that frontal frequency and frontal density have increased in both regions in the past three decades, by around 0.2–0.3%. In addition, both regions exhibit higher frequency and density of fronts in austral winter and fewer in austral summer. Our calculations show that changes in frontal frequency/density show some relationship to El Niño-Southern Oscillation and Indian Ocean Dipole. Changes in frontal activity could strongly impact local ocean biogeochemistry and marine ecosystems. A better understanding changing fronts in hotspots will help predict and manage future changes in regional oceans to warming.

Keywords Oceanic fronts · Satellite imagery · Remote sensing · Southeast Australia (25°–43° S, 146°–161° E) · Southwest Australia (21°–43° S, 88°–116° E)

Abbreviations

Fd   Frontal density
Ff   Frontal frequency

✉ Kai Yang
   kai.yang@utas.edu.au

   Andrew M. Fischer
   andy.fischer@utas.edu.au

   Pallavi Govekar
   pallavi.govekar@bom.gov.au

1 Institute for Marine and Antarctic Studies, University of Tasmania, Launceston 7250, Australia

2 Australian Research Council Centre of Excellence for Climate Extremes, Canberra Airport ACT 2609, Australia

3 Australian Bureau of Meteorology, VIC 3008, Australia

1 Introduction

Two contiguous masses of water separated by a front typically have distinct physical, biological, and visual properties. At fronts, convection occurs, mixing intensifies, and turbulence increases. Numerous factors, including bathymetry (Wolanski and Hamner 1988) and various atmospheric and oceanic conditions, influence the variability of fronts (Belkin et al. 2009). Consequently, several mechanisms, including eddy fields, boundary currents, and upwelling, contribute to front formation (Belkin 2021) leading to fronts that vary in size from a few kilometres to tens of thousands of kilometres and can be transient or seasonal events across a variety of time scales (Joseph 2014, 2017).

Near fronts, water masses are mixed through the process of convergence or divergence. Water movement and mixing may increase biological activity along fronts by transferring nutrients (Sato et al. 2018). The increase in biological activity has further effects on marine ecosystems (Brandini et al. 2018), altering the composition of plankton communities and the related biogeochemical fluxes (Landry et al. 2012; Stukel et al. 2017). Additionally, fronts also influence

ecosystem productivity and species distributions (Woodson and Litvin 2015), such as the Atlantic bluefin tuna (*Thunnus thynnus*; Royer et al. 2004) and the Pacific albacore tuna (*Thunnus alalunga*; Xu et al. 2017). By directing nutrients via alternate trophic pathways, fronts may increase ecosystem biomass and fisheries yield (Woodson and Litvin 2015). Oceanic fronts are prevalent in upwelling systems (Mauzole et al. 2020) and play a significant role in predator–prey interactions and energy transmission throughout food webs (Sato et al. 2018), hence increasing the quantity of forage fish and top predators (Snyder et al. 2017). Fronts have a substantial influence on exchanges between the ocean, atmosphere, and cryosphere and are of basic importance to the climate system (Chapman et al. 2020; Sallée et al. 2008; Williams et al. 2007).

In recent decades, it has become more evident that climate change may have an impact on the frontogenesis or the formation of fronts. Kahru et al. (2012) analysed frontal trends in the California Current System and determined that frontal frequency has increased over time. In addition, Kahru et al. (2018) focused on the impact of warm anomalies in the North–East Pacific from 2014 and 2016. It was suggested that warm anomalies considerably reduced the frequency of fronts (Kahru et al. 2018). Also, along the Central Chilean coast, Oerder et al. (2018), observed an increasing trend in frontal frequency. In addition, a global analysis of fronts revealed a long-term increase in front probability, although this trend was not uniform across the entire ocean (Obenour 2013).

Hobday and Pecl (2014) identified 24 ocean warming hotspots, regions that are warming faster than 90 percent of the global ocean. The consequences of ocean warming on ecosystems will likely be noticed early in these hotspots. For instance, García-Reyes and Largier (2010) confirmed the hypothesis of Bakun (1990) that global warming will exacerbate coastal upwelling circulation by amplifying alongshore winds because of greater onshore–offshore atmospheric-pressure gradients. This could have led to the enhanced front probability observed by Obenour (2013) and is more likely to be observed in ocean warming hotspots. A recent study highlighted general trends in frontal activity across various hotspots in the global ocean (Yang et al. 2023). However, a focused investigation into specific regions is crucial for understanding the local environment and its impact on the economy.

Given the conflicting results of previous studies (e.g., Kahru et al. 2012, 2018) and the variability of changes to frontal frequency across the globe, it is increasingly important to examine trends of frontal frequency within the context of a changing (warming) ocean. Changes to regional productivity due to changes in frontal frequency are likely to have impacts on ecosystem productivity and as a result, local economies. Given that temperate Australia is experiencing ocean warming two to four times faster than the global average (Lough and Hobday 2011; Pearce and Feng 2007), we focused on the two ocean warming hotspots near Australia. In this study, we aim to characterize changes of frontal activity (including long-term trends, seasonal variability, and temporal spatial distribution of frontal trends) within the two hotspots.

2 Data and Methods

2.1 Study Area

The study areas are located in southeast Australia (hereafter referred to as SEA; 25°–43° S, 146°–161° E) and southwest Australia (hereafter referred to as SWA; 21°–43° S, 88°–116° E; blue areas in Fig. 1). These areas are selected
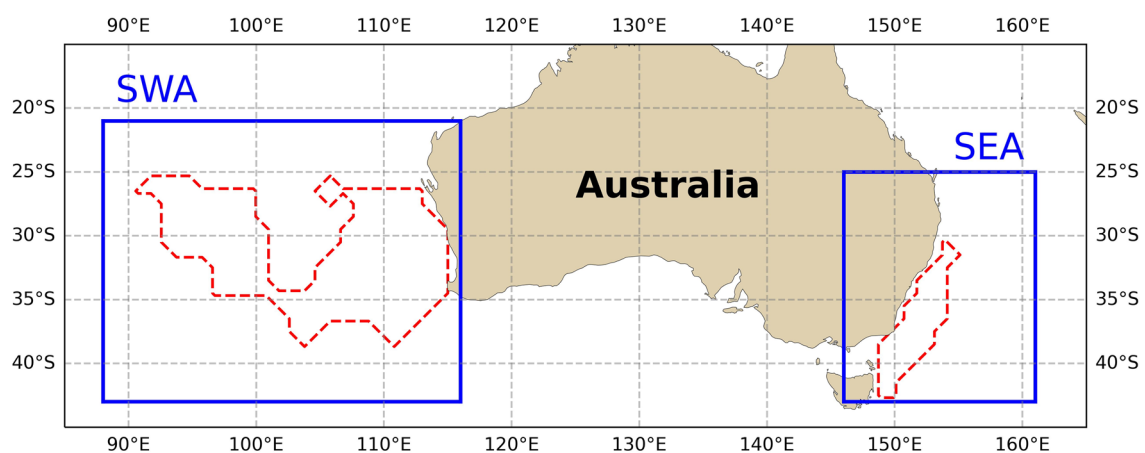

Fig. 1 Study areas: southwest Australia (SWA; 21°–43° S, 88°–116° E) and southeast Australia (SEA; 25°–43° S, 146°–161° E) regions, marked by solid blue lines. Dotted red lines highlight the two ocean warming hotspots near Australia, according to Hobday and Pecl (2014)

for covering two ocean warming hotspots defined by Hobday and Pecl (2014; red areas in Fig. 1). According to previous studies (Hobday and Pecl 2014; Ridgway 2007), the SEA hotspot is warming up to four times faster than the global average. The SEA region is strongly influenced by the East Australian Current (EAC), which flows south along the eastern seaboard. The EAC carries tropical water south and retroflects towards the east. The retroflection of the EAC forms the Tasman Front, south of which are cool, sub-Antarctic waters. The diverse ecology and biology are also one of the features of the southeast Australia (Curley et al. 2013). Warming in this hotspot is partly caused by the strengthening and poleward shift of the EAC (Hill et al. 2008; Ridgway 2007; Ridgway and Dunn 2003). The poleward shift of several dozen marine species was found to be related to the variations of the EAC (Johnson et al. 2011; Last et al. 2011). This kind of species invasion could have negative effects on the structure and function of the ecosystems of areas in the south, such as coastal Tasmania (Marzloff et al. 2016).

The SWA study area covers the southwest Australia continental shelf and part of the southeast Indian Ocean (Fig. 1). This area is strongly influenced by the Leeuwin Current (LC). The LC is an eastern boundary current of the southern Indian Ocean that flows southward off the western seaboard of Australia. Along the coast of Western Australia, the western rock lobster is the basis of Australia's most valuable fishery. The local western rock lobster fishery is influenced by the strength of the LC, water temperatures, and the westerly winds (Caputi et al. 2003).

2.2 Satellite SST Data

We used a 6-day composite SST product in this study to detect fronts. The 6-day night-time L3S SST product with a high spatial resolution ($0.02° \times 0.02°$) was obtained from the Australian Ocean Data Network (AODN) Thredds server http://thredds.aodn.org.au/thredds/catalog/IMOS/SRS/SST/ghrsst/catalog.html. The diurnal warming can enhance SST by more than 3 degrees under the calm and clear conditions and can produce noise to the daily SST observations (Kawai and Kawamura 2002; Wirasatriya et al. 2020). To avoid the issue of potential diurnal warming during the daytime, only night-time SSTs are used. The 6-day night L3S SST is the 6-night average of all the highest quality retrieved "skin" SSTs of the ocean at approximately 10–20 μm depth, based on all contributing pixels to the cell, weighted by the area of overlap. For the period of 1st January 1993–31st December 2011, AVHRR-only 6-day L3S product was used. The 6-day Multi-sensor L3S SST product was used to obtain more high-quality and accurate data from 1 January 2012 to 31 December 2019. Both datasets are SST skin products and provide $0.02° \times 0.02°$ spatial resolution. To ensure the best quality and highest accuracy, we subtracted sses_bias from

each SST value and only used quality level 4 and 5 data, following guidelines of GHRSST file conventions (GHRSST Science Team 2010).

2.3 Detection of Oceanic Fronts

Remotely sensed imagery is widely used for detecting oceanic fronts. Sea surface temperature (SST) derived from satellite radiance values determine gradients in sea surface temperature from which frontal locations can be derived. Several methods have been proposed to extract frontal information from satellite imagery, including various edge detection algorithms. These algorithms range from simple edge operators for characterizing horizontal gradients of a field (Canny 1986) to more sophisticated algorithms such as cluster-shade analysis (Holyer and Peckinpaugh 1989), histogram analysis (Cayula and Cornillon 1992; Saraceno et al. 2005), entropy analysis based on the Jensen-Shannon divergence (Vázquez et al. 1999), and semivariogram analysis (Diehl et al. 2002).

In this study, oceanic fronts were detected using the Cayula and Cornillon algorithm (Cayula and Cornillon 1992, 1995). This algorithm was initially developed for SST imagery and has gained wide popularity. Numerous studies have used it to map SST fronts globally and locally (Belkin et al. 2009; Kahru et al. 2012; Sarkar et al. 2019; Ullman and Cornillon 1999). Within a detecting window of a front separating two water masses, a histogram of SST values of all pixels would always contain two modes corresponding to the two water masses, whereas the front is a locus of SST values that correspond to a minimum between the two modes. A vital advantage of this algorithm is its independence on specific gradient strengths or isolines. This allows it to provide objective frontal detection results. Examples of the images of the fronts detected using the Cayula and Cornillon algorithm in the two regions are shown in Fig. 2a, d.

The Cayula and Cornillon algorithm was applied by using the Marine Geospatial Ecology Tools (MGET), version 0.8a75, released 8 April 2021 (Cayula and Cornillon 1992; Roberts et al. 2010).

2.4 Metrics

Two metrics were used to characterize frontal activity; frontal density reflects the percentage of an area occupied by frontal pixels, while frontal frequency represents the total presence of fronts in the area throughout time in terms of frequency.

After applying the frontal detection algorithm, each SST frontal image contains only three kinds of pixels: invalid pixels (pixel value = NaN), frontal pixels (pixel value = 1) and non-frontal pixels (pixel value = 0). For each map, frontal density (Fd), the ratio between the number of frontal pixels
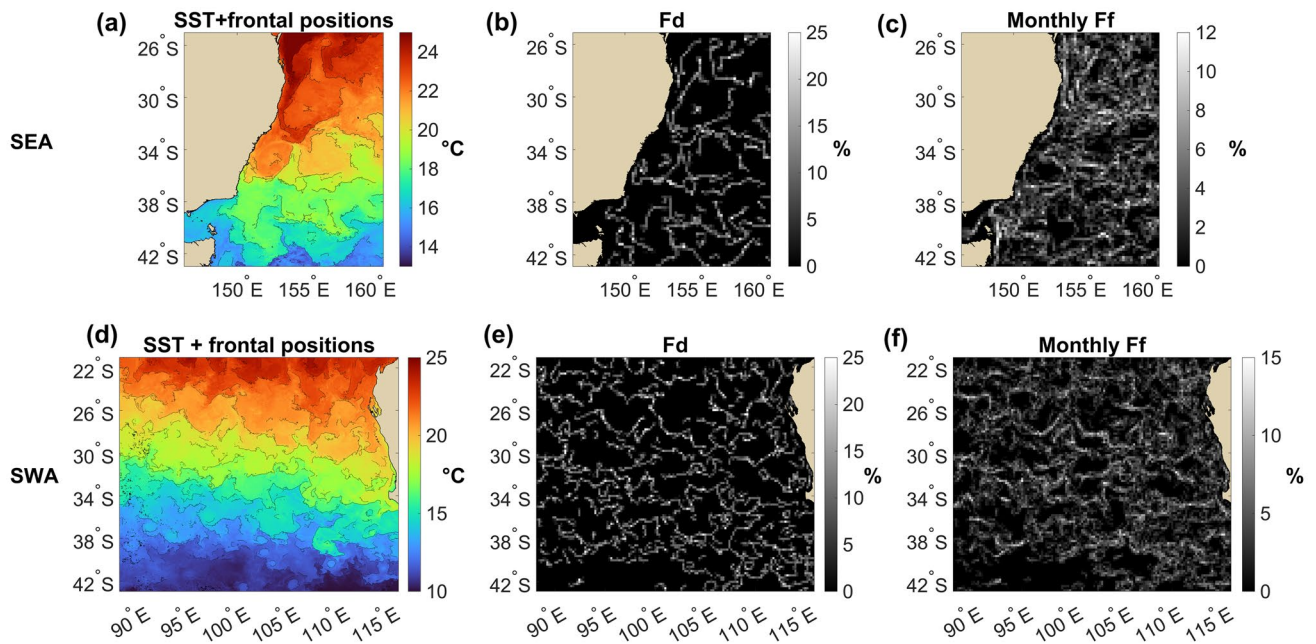
Fig. 2 Southeast Australia (SEA) region and Southwest (SWA) Australia hotspot are used to illustrate frontal detection and frontal characteristics: **a**, **d**, snapshot of observed frontal positions (thin black lines) overlapping 6-day averaged sea surface temperature (SST) values (SEA: 06 May 2012–11 May 2012; SWA: 03 Sep 2012–08 Sep 2012); **b**, **e**, spatial patterns of frontal density (Fd) of (**a**) and (**d**); **c**, **f**, resampled spatial patterns of monthly frontal frequency (Ff; SEA: May 2012; SWA: September 2012). Fd is calculated with a 10×10 pixels window

($n_{\mathrm{front,}}$ pixel value $= 1$) and the total number of all valid pixels (n_{valid}, pixel value $= 0$ and 1) (Eq. 1) was calculated. The unit of Fd used in this study is the percentage of the entire area (%) occupying fronts within a region. We obtained one Fd value for each satellite image based on this definition. Because SST data are 6-day composites, the time step of the Fd time series is also 6 days. By averaging the time series, we obtained monthly Fd time series. Spatial patterns of Fd are calculated within a 10×10 pixels window. Examples of the Fd images are shown in Fig. 2b and e for both regions.

$$\mathrm{Fd} = n_{\mathrm{front}}/n_{\mathrm{valid}} \qquad (1)$$

Fd: the spatial proportion of fronts or frontal density, n_{front}: the number of frontal pixels (pixels with value 1) within a frontal image, n_{valid}: the number of valid pixels (pixels with values 0 and 1) within a frontal image.

Secondly, frontal frequency (Ff) was used to represent the likelihood of the occurrence of fronts over a specific period. It is the ratio between the accumulation of the counts of frontal detections and valid detections over a given time interval (Eq. 2). In this study, we used one month as the time interval to calculate Ff. For each month, there are five 6-day composite SST images. We focus on a pixel in the same location of the five SST images (taken within a month). Assuming that each of the five pixels has a valid SST value rather than NaN ($N_{\mathrm{valid}} = 5$) and that three of them are

defined as frontal pixels ($N_{\mathrm{front}} = 3$), Ff during the month is 0.60 or 60%. During the study, this computation was applied to each pixel, resulting in one Ff map per month. By taking average for each Ff map, we obtained monthly time series of Ff. Examples of the Ff images are shown in Fig. 2c and f for both regions.

$$\mathrm{Ff} = N_{\mathrm{front}}/N_{\mathrm{valid}} \qquad (2)$$

Ff: the frequency of frontal detections for an individual pixel over a given time interval, N_{front}: the accumulation of the counts of front detections over a given time interval, N_{valid}: the accumulation of the counts of valid detections over a given time interval.

The annual mean cycles of Fd and Ff were computed by averaging the monthly composites for each variable. By subtracting the mean annual cycle from the appropriate time series, the corresponding monthly anomalies were computed.

2.5 Trends, Significance, and Uncertainties

The trend analysis of this study is consistent with the analysis used by Martínez-Moreno et al. (2021). For spatially integrated time series, linear trends are calculated using linear least-squares regression. For the trend maps, the fields are first coarsened to a $0.2° \times 0.2°$ grid, and then the linear

trends are computed for each grid point. All the observed trends for anomalies of SST, Fd, and Ff (time-series and trend maps) are assessed using the Theil–Sen estimator. A modified Mann–Kendall test (Yue and Wang 2004) is used to assess the statistical significance of trends. Furthermore, uncertainties of trends are calculated by dividing the standard deviation of the time series by the square root of the effective sample size from the Mann–Kendall test.

3 Results

3.1 Temporal Trends of SST Fronts

Both regions exhibit statistically significant positive trends in Ff and Fd (Fig. 3d and 2e; Table 1). For the SEA region, Ff anomaly increases at a rate of 0.230% ± 0.070% per decade, while Fd anomaly increases at a rate of 0.227 ± 0.070% per decade (red curves and bars in Fig. 3d and e; Table 1). Increases in anomalies of both Ff and

Table 1 Linear trends for frontal frequency (Ff, %/decade), frontal density (Fd, %/decade), and sea surface temperature (SST, °C/decade) anomalies, for the southeast Australia (SEA) and southwest Australia (SWA) hotspot regions

Region	Ff	Fd	SST
SEA	+0.230±0.070*	+0.227±0.070*	+0.304±0.038*
SWA	+0.290±0.077*	+0.272±0.073*	+0.029±0.086

*, statistically significant at the 95% confidence level. Linear trends are calculated using linear least-squares regression. Statistical significance of trends are accessed using a modified Mann–Kendall test (See methods)

Fd are slightly higher in the SWA region, 0.290 ± 0.077% and 0.272 ± 0.073% per decade, respectively (blue curves and bars in Fig. 3d and e; Table 1). For comparison, both hotspot regions exhibit positive SST anomaly trends from 1993 to 2019, positively correlated with trends in Ff and Fd.
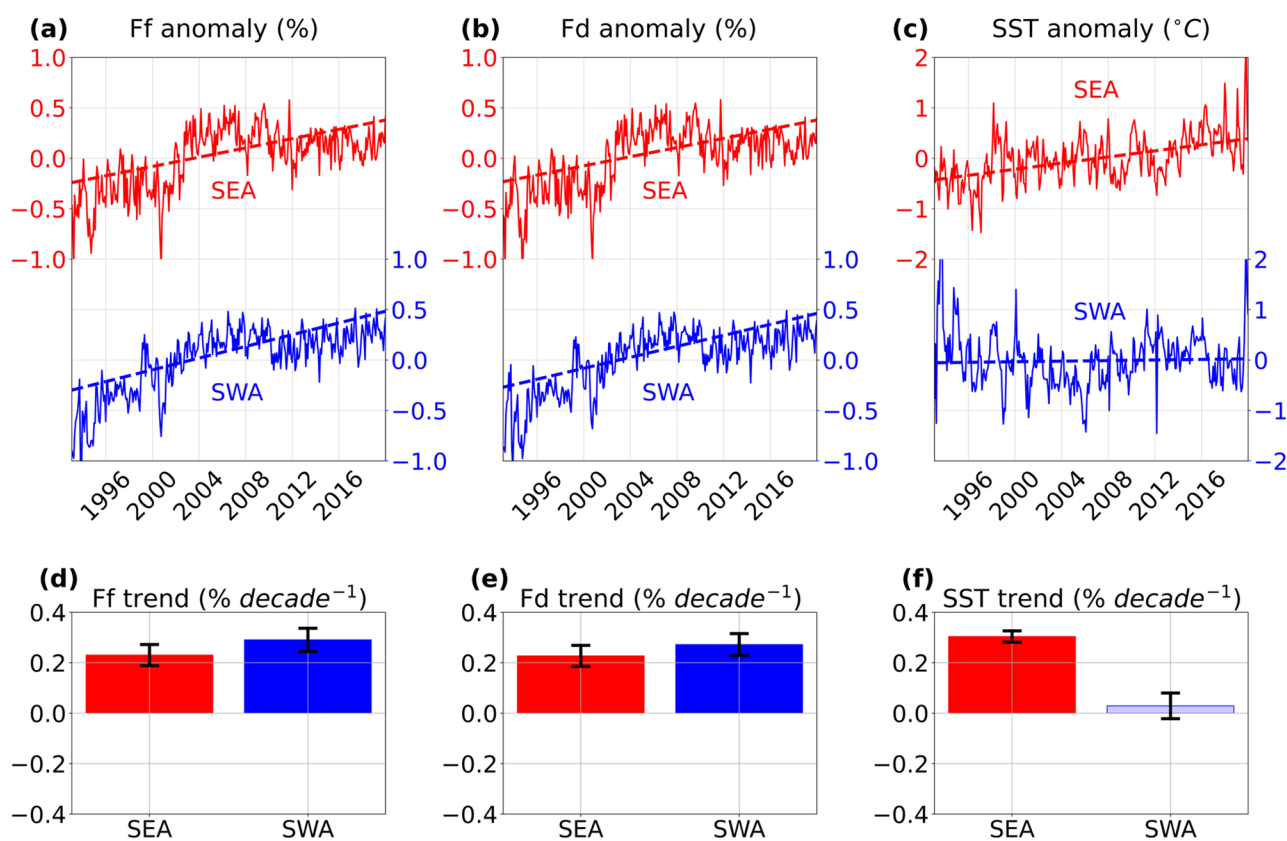

Fig. 3 Time-series and linear trends for southeast Australia (SEA; red) and southwest Australia (SWA; blue). **a** Frontal frequency (Ff) anomaly, **b** frontal density (Fd) anomaly, **c** SST anomaly. Solid lines represent monthly running average for each region; the dashed lines correspond to time-series trends; **d** linear Ff anomaly trends for each region, **e** linear Fd anomaly trends, and **f** linear SST anomaly trends.

In **d**–**f**, statistically significant trends (above the 95% confidence level) are solid bars, while non-significant trends are translucent; standard errors are shown with black error bars. Linear trends are calculated using linear least-squares regression. Statistical significance of trends is accessed using a modified Mann–Kendall test (See Methods)

3.2 Spatial Distributions of Frontal Trends

The maps of Ff and Fd anomaly trends show increasing patterns in the southeast portion of the SEA region, where both Ff and Fd increases at rates over 0.5% per decade (dark red patterns in Fig. 4a). In addition, three locations with positive Ff and Fd trends exceeding +0.5% per decade were also found along the continental shelf: near the Brisbane and Sydney coasts, and in the Bass Strait (red arrows in Fig. 4a and b). Patterns indicating decreasing Ff and Fd were observed in the middle of the SEA region and close to Cape Howe (the blue arrow in Fig. 4a and b). Geographically, however, the patterns of rapidly increasing SST are not consistent with the patterns of either increasing or decreasing Ff and Fd.

Spatial patterns of increasing Ff and Fd of over 0.5% per decade are evenly distributed throughout the SWA region (dark red patterns in Fig. 5a and b) and are more concentrated in the central and eastern areas. Compared with the SST anomaly trends (Fig. 5c), there appears to be a limited degree of co-occurrence between SST and Ff (or Fd) anomalies.

3.3 Mean Annual Cycle of SST Fronts

For both hotspot regions, the mean annual cycles in Ff and Fd are identical and coincide with cycles of SST (Fig. 6).

In the SEA region, the mean annual cycles of Ff and Fd are coincided and have bimodal patterns (Fig. 6a, c). The maximum of Ff and Fd occurs in late winter or early spring (September and October), while the second maximum of Ff and Fd occurs in early autumn (March and April) (Fig. 6a, c). In the SWA region, the maximum for Ff and Fd occurs in late winter or spring (August) (Fig. 6b, d).

4 Discussion and Conclusion

Increasing trends of Ff and Fd in the two hotspot areas of Australia suggest changes to features and processes of the ocean surface. Changes in the global climate system and recent warming of the upper ocean have strengthened and accelerated ocean currents and the intensified wind stress (Martínez-Moreno et al. 2021). For the SEA region, changes of frontal characteristics could attribute to the poleward shift of the EAC (Ridgway and Dunn 2003; Oke et al. 2019). The current accelerates and deepens as it moves poleward (Ridgway and Dunn 2003). This drives more warmer waters from the low latitudes into the SEA region. Sharp gradients on the sea surface may become more pronounced. In other words, stronger fronts become more detectable by the algorithm. Changes in frontal characteristics in the SWA region, which encompasses a vast area off the western coast of Australia, may be associated with several complicated processes.
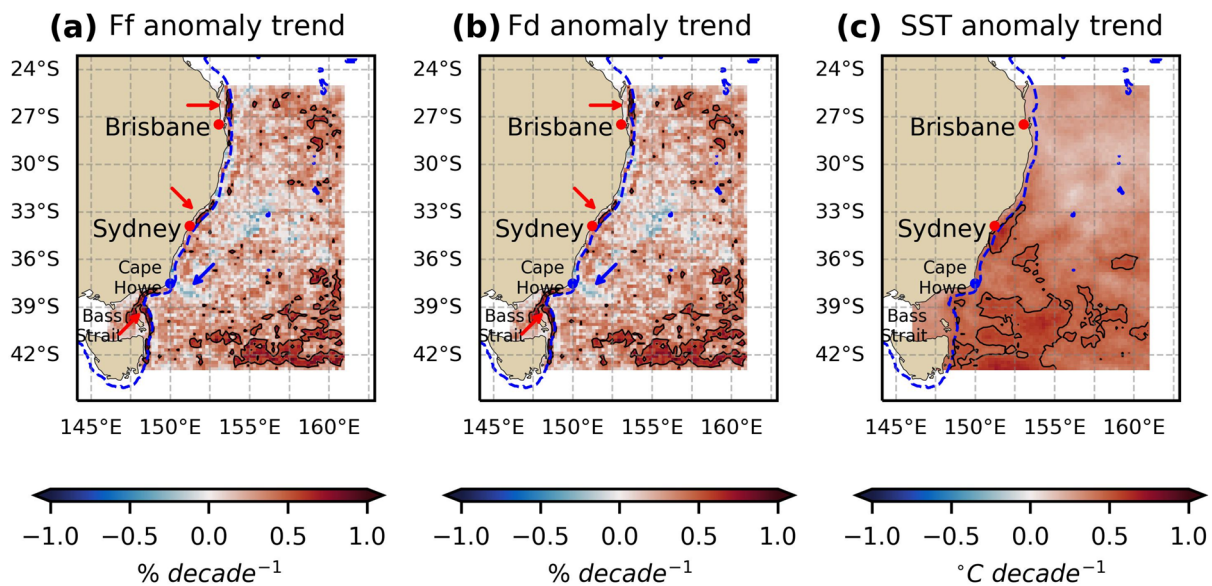

Fig. 4 Regional maps of **a** frontal frequency (Ff), **b** frontal density (Fd), and **c** sea surface temperature (SST) trends in the southeast Australia (SEA) region. Solid contours show positive trends (contours of +0.5 °C per decade for SST, +0.5% per decade for Ff and Fd). The dotted blue contours indicate the 200 m isobath. In **b** and **c**, red arrows highlight the three zonal areas near the Australian coast with strong positive trends near the Brisbane and Sydney coasts, and the Bass Strait. The blue arrow points to coastal areas near Cape Howe, with negative trends for Ff and Fd. For Ff, Fd, and SST maps, the fields are first coarsened to a 0.2° × 0.2° grid, and then the linear trends are computed for each grid point
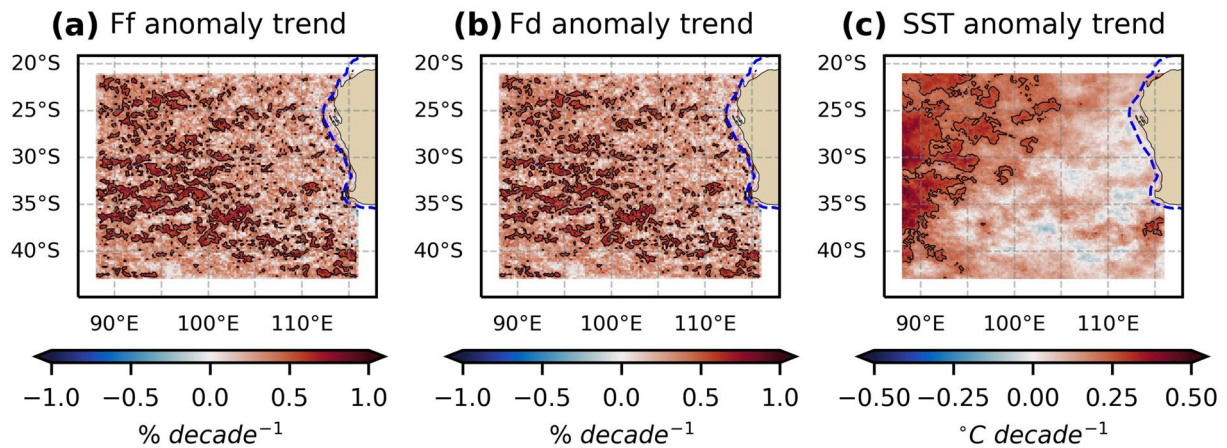
Fig. 5 Regional trends of **a** frontal frequency (Ff), **b** frontal density (Fd), and **c** sea surface temperature (SST) anomalies in the southwest Australia (SWA) hotspot. The solid contours show positive trends (contours of +0.25 °C per decade for SST, +0.5% per decade for Ff and Fd). The dotted blue contours indicate the 200 m isobath. For Ff, Fd, and SST maps, the fields are first coarsened to a 0.2°×0.2° grid, and then the linear trends are computed for each grid point

Fig. 6 Mean annual cycles of monthly frontal frequency (Ff) and frontal density (Fd) in the southeast Australia (SEA) hotspot, as shown in (**a**) and (**c**); and the southwest Australia (SWA) hotspots, as shown in (**b**) and (**d**). The annual mean cycles of Fd and Ff were computed by averaging the monthly composites for each variable
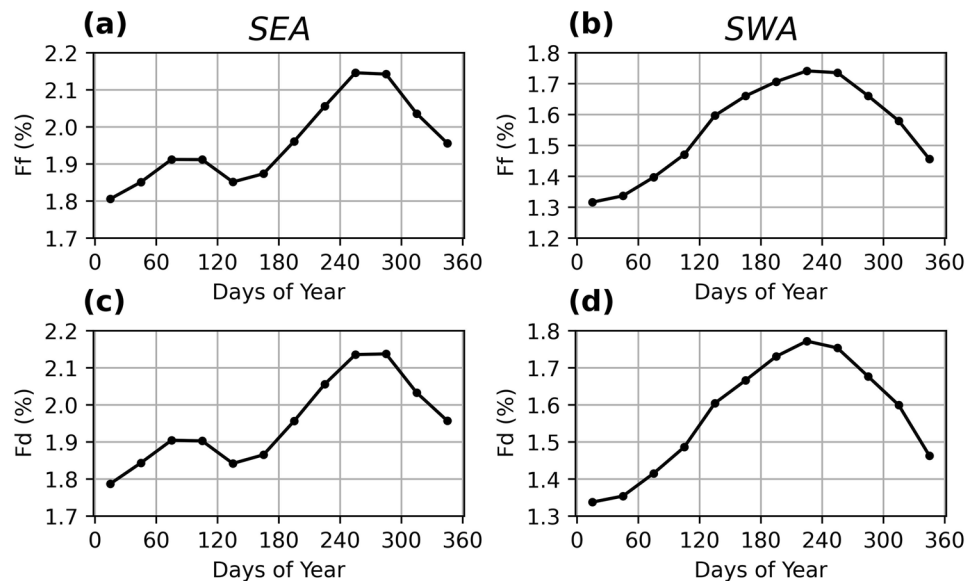
To further explore the drivers of frontal variability, we calculated the correlation coefficient between our time series of frontal activity and time series of two key atmospheric and oceanic variables influencing Australian climate: the Southern Oscillation Index (SOI) and the Indian Ocean Dipole (IOD) index (Fig. 7). For both hotspot regions, there is a weak positive correlation between frontal activity (Ff and Fd) and SOI and a weak negative correlation between frontal activity and IOD index. Specifically, the frequency and density of frontal activity has the potential to increase during La Niña and/or negative IOD events. La Niña is often associated with negative IOD events, and both tend to result in above-average precipitation and below-average temperatures across most of mainland Australia south of the tropics (Bureau of Meteorology 2023). These changes may result in cooler water in coastal regions. In addition, previous research suggested that both EAC and LC enhanced during La Niña (Pattiaratchi and Siji 2020). Thus, for both studied hotspot regions, SST difference between cooler coasts and enhanced ocean currents (warmer) is potentially increased during La Niña, which has the potential to elevate frontal activity (Pattiaratchi and Siji 2020). Given the connection between ENSO and IOD events, negative IOD events also tend to be accompanied by an increase in fronts.

Seasonal variability of frontal activity was observed in both hotspot regions (Fig. 6). Both regions exhibit higher
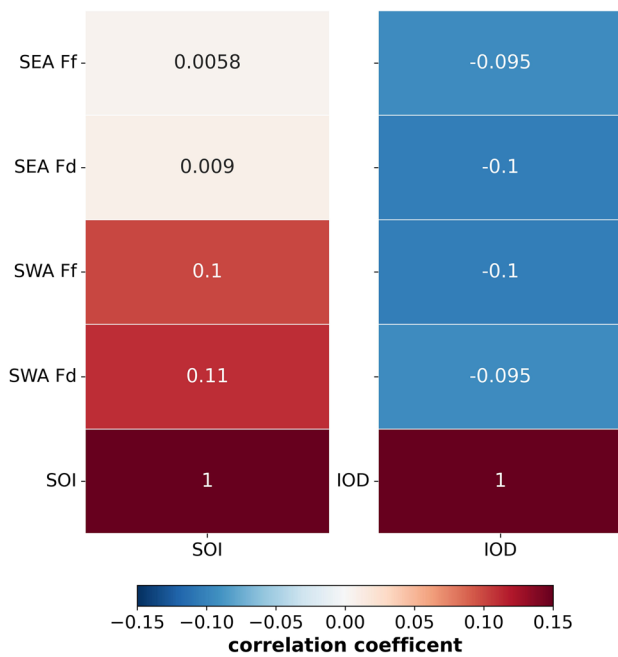
Fig. 7 Correlation heatmap between detrended time series of frontal activity and timeseries of the Southern Oscillation Index (SOI)/ the Indian Ocean Dipole (IOD) index. SEA, the southeast Australia region; SWA, the southwest Australia region; Ff, frontal frequency time series; Fd, frontal density time series

Ff and Fd in late winter and early spring (August–October) and decreased Ff and Fd in austral summer months (December–February; Fig. 6). It has been proposed that fronts are closely related with mesoscale eddies (Mauzole et al. 2020). Studies show a maximum EAC transport of 21.6 ± 1.4 Sv at 26° S in March, and a minimum transport of 18 ± 1.4 Sv in August (Zilberman et al. 2018). The stronger EAC flow in summer is associated with higher eddy kinetic energy (EKE) in the Tasman Sea (Qiu and Chen 2004), and according to Liu et al. (2022), surface EKE in the EAC averaged in 148 E–160 E, 30 S–45 S reached a maximum in February and then gradually fell until it reached a minimum in August. The results here show that increased EKE in February/March is associated with a minimum Ff and Fd in the SEA hotspot, indicating that frontal strength may be decreasing with increasing EKE and are not being detected across the temperature threshold of the algorithm. Conversely, a decrease in EKE may be associated with increased frontal strength and detection of fronts in August. For the SWA region, the LC was confirmed to have significant seasonal cycles, weakest in the austral summer and strongest in the austral winter. (Akhir et al. 2020; Feng et al. 2003, 2009; Ridgway and Godfrey 2015). This coincides with our observation of the mean annual cycle of Ff and Fd in the SWA region. In near-shore waters, the dynamics of upwelling were found to control the spatio-temporal variability of productivity (Waite

et al. 2007). Generally strong and persistent southerlies during the summer months generate "upwelling favourable" conditions and the development of upwelling fronts. However, this seasonal upwelling process is largely suppressed by the southward-flowing Leeuwin Current, which increases in the autumn and winter and when the southerlies are less consistent and are more variable (Pattiaratchi and Woo 2009). These results indicate a longer term decrease in Ff and Fd closer to shore highlighting the potential decrease in upwelling fronts related to a decrease in nearshore upwelling favourable wind stress in winter (−4.2%) (Foster and Sudmeyer 2021). Changes in fronts related to upwelling could influence local fisheries. For example, according to Australian Commonwealth fisheries, the SEA region comprises key species groupings such as tuna, billfish, scalefish, and shark. Reduced upwelling fronts may result in decreasing fish catch (Wen et al. 2023).

Fd and Ff exhibit consistency in all aspects of our results, indicating a strong correlation between the two metrics. Frequent frontal activity would logically correspond to many fronts. However, this does not imply that the two metrics are equivalent. There is an essential difference between them; Ff indicates the presence of frontal activity in the time dimension, i.e., whether fronts are always present; while Fd quantifies the quantity of frontal activity in the spatial dimension, i.e., the number of frontal pixels. The correlation between the two metrics requires further investigation.

The main result of this study is the overall increase of frontal activity (in frequency and density) within two hotspot areas of Australia over the past 3 decades. The observed changes in frontal activity have the potential to influence regional ocean circulation and air–sea exchange of heat, carbon, etc. The results of frontal activity seasonal cycles and geographic trends' patterns provide background for future research on fronts within other hotspots or any regional-scale area. Our findings thus are important for investigating future changes in sea surface to a changing climate.

Declarations

Conflict of interest The authors declare no competing interests.

References

Akhir MF, Pattiaratchi C, Meuleners M (2020) Dynamics and seasonality of the Leeuwin current and the surrounding counter-current system in the region south of Western Australia. J Mar Sci Eng 8(8):552. https://doi.org/10.3390/jmse8080552

Bakun A (1990) Global climate change and intensification of coastal ocean upwelling. Science 247(4939):198–201. https://doi.org/10.1126/science.247.4939.198

Belkin IM (2021) Remote sensing of ocean fronts in marine ecology and fisheries. Remote Sens-Basel 13(5):883. https://doi.org/10.3390/rs13050883

Belkin IM, Cornillon PC, Sherman K (2009) Fronts in large marine ecosystems. Prog Oceanogr 81(1–4):223–236. https://doi.org/10.1016/j.pocean.2009.04.015

Brandini FP, Tura PM, Santos PP (2018) Ecosystem responses to biogeochemical fronts in the South Brazil Bight. Prog Oceanogr 164:52–62. https://doi.org/10.1016/j.pocean.2018.04.012

Bureau of Meteorology (2023) The Indian ocean dipole (IOD). http://www.bom.gov.au/climate/enso/history/ln-2010-12/IOD-what.shtml. Accessed 1 Feb 2023

Canny J (1986) A computational approach to edge detection. IEEE T Pattern Anal 6:679–698. https://doi.org/10.1109/TPAMI.1986.4767851

Caputi N, Chubb C, Melville-Smith R, Pearce A, Griffin D (2003) Review of relationships between life history stages of the western rock lobster, Panulirus Cygnus, in Western Australia. Fish Res 65(1–3):47–61. https://doi.org/10.1016/j.fishres.2003.09.006

Cayula JF, Cornillon P (1992) Edge detection algorithm for SST images. J Atoms Ocean Tech 9(1):67–80. https://doi.org/10.1175/1520-0426(1992)009%3c0067:EDAFSI%3e2.0.CO;2

Cayula JF, Cornillon P (1995) Multi-image edge detection for SST images. J Atoms Ocean Tech 12(4):821–829. https://doi.org/10.1175/1520-0426(1995)012%3c0821:MIEDFS%3e2.0.CO;2

Chapman CC, Lea MA, Meyer A, Sallée JB, Hindell M (2020) Defining southern ocean fronts and their influence on biological and physical processes in a changing climate. Nat Clim Change 10(3):209–219. https://doi.org/10.1038/s41558-020-0705-4

Curley BG, Jordan AR, Figueira WF, Valenzuela VC (2013) A review of the biology and ecology of key fishes targeted by coastal fisheries in south-east Australia: identifying critical knowledge gaps required to improve spatial management. Rev Fish Biol Fisher 23(4):435–458. https://doi.org/10.1007/s11160-013-9309-7

Diehl SF, Budd JW, Ullman D, Cayula JF (2002) Geographic window sizes applied to remote sensing sea surface temperature front detection. J Atoms Ocean Tech 19(7):1105–1113. https://doi.org/10.1175/1520-0426(2002)019%3c1105:GWSATR%3e2.0.CO;2

Feng M, Meyers G, Pearce A, Wijffels S (2003) Annual and interannual variations of the Leeuwin current at 32 S. J Geophys Res-Oceans 108(C11):3355. https://doi.org/10.1029/2002JC001763

Feng M, Waite AM, Thompson PA (2009) Climate variability and ocean production in the Leeuwin current system off the west coast of Western Australia. J R Soc West Aust 92:67

Foster I, Sudmeyer R (2021) Wind speed is projected to remain unchanged. https://www.agric.wa.gov.au/climate-change/climate-projections-western-australia. Accessed 20 Jun 2023

García-Reyes M, Largier J (2010) Observations of increased wind-driven coastal upwelling off central California. J Geophys Res-Oceans 115(C4):C04011. https://doi.org/10.1029/2009JC005576

GHRSST Science Team (2010) The recommended GHRSST data specification (GDS) 2.0, document revision 4. GHRSST International Project Office. https://www.ghrsst.org/wp-content/uploads/2021/04/GDS20r5.pdf. Accessed 1 Feb 2023

Hill KL, Rintoul SR, Coleman R, Ridgway KR (2008) Wind forced low frequency variability of the East Australia current. Geophys Res Lett 35(8):L08602. https://doi.org/10.1029/2007GL032912

Hobday AJ, Pecl GT (2014) Identification of global marine hotspots: sentinels for change and vanguards for adaptation action. Rev Fish Biol Fisher 24(2):415–425. https://doi.org/10.1007/s11160-013-9326-6

Holyer RJ, Peckinpaugh SH (1989) Edge detection applied to satellite imagery of the oceans. IEEE T Geosci Remote 27(1):46–56. https://doi.org/10.1109/36.20274

Johnson CR, Banks SC, Barrett NS, Cazassus F, Dunstan PK, Edgar GJ, Frusher SD, Gardner C, Haddon M, Helidoniotis F, Hill KL (2011) Climate change cascades: shifts in oceanography, species' ranges and subtidal marine community dynamics in eastern Tasmania. J Exp Mar Biol Ecol 400(1–2):17–32. https://doi.org/10.1016/j.jembe.2011.02.032

Joseph A (2014) Oceanic currents and their implications. In: Joseph A (ed) Measuring ocean currents. Elsevier, Boston, pp 1–49

Joseph A (2017) Magic with colors sea surface changes. In: Joseph A (ed) Investigating seafloors and oceans. Elsevier, Amsterdam, pp 555–574

Kahru M, Di Lorenzo E, Manzano-Sarabia M, Mitchell BG (2012) Spatial and temporal statistics of sea surface temperature and chlorophyll fronts in the California Current. J Plankton Res 34(9):749–760. https://doi.org/10.1093/plankt/fbs010

Kahru M, Jacox MG, Ohman MD (2018) CCE1: decrease in the frequency of oceanic fronts and surface chlorophyll concentration in the California current system during the 2014–2016 northeast Pacific warm anomalies. Deep-Sea Res Pt I 140:4–13. https://doi.org/10.1016/j.dsr.2018.04.007

Kawai Y, Kawamura H (2002) Evaluation of the diurnal warming of sea surface temperature using satellite-derived marine

meteorological data. J Oceanogr 58(6):805–814. https://doi.org/10.1023/A:1022867028876

Landry MR, Ohman MD, Goericke R, Stukel MR, Barbeau KA, Bundy R, Kahru M (2012) Pelagic community responses to a deep-water front in the California current ecosystem: overview of the A-front study. J Plankton Res 34(9):739–748. https://doi.org/10.1093/plankt/fbs025

Last PR, White WT, Gledhill DC, Hobday AJ, Brown R, Edgar GJ, Pecl G (2011) Long-term shifts in abundance and distribution of a temperate fish fauna: a response to climate change and fishing practices. Global Ecol Biogeogr 20(1):58–72. https://doi.org/10.1111/j.1466-8238.2010.00575.x

Liu J, Zheng S, Feng M, Xie L, Feng B, Liang P, Wang L, Yang L, Yan L (2022) Seasonal variability of eddy kinetic energy in the East Australian current region. Front Mar Sci 9:1069184. https://doi.org/10.3389/fmars.2022.1069184

Lough JM, Hobday AJ (2011) Observed climate change in Australian marine and freshwater environments. Mar Freshwater Res 62(9):984–999. https://doi.org/10.1071/MF10272

Martínez-Moreno J, Hogg AM, England MH, Constantinou NC, Kiss AE, Morrison AK (2021) Global changes in oceanic mesoscale currents over the satellite altimetry record. Nat Clim Change 11(5):397–403. https://doi.org/10.1038/s41558-021-01006-9

Marzloff MP, Melbourne-Thomas J, Hamon KG, Hoshino E, Jennings S, Van Putten IE, Pecl GT (2016) Modelling marine community responses to climate-driven species redistribution to guide monitoring and adaptive ecosystem-based management. Glob Change Biol 22(7):2462–2474. https://doi.org/10.1111/gcb.13285

Mauzole YL, Torres HS, Fu LL (2020) Patterns and dynamics of SST fronts in the California current system. J Geophys Res-Oceans 125(2):2019JC015499. https://doi.org/10.1029/2019JC015499

Obenour KM (2013) Temporal trends in global sea surface temperature fronts. Ph.D. Thesis, University of Rhode Island, p 46

Oerder V, Bento JP, Morales CE, Hormazabal S, Pizarro O (2018) Coastal upwelling front detection off central Chile (36.5–37 S) and spatio-temporal variability of frontal characteristics. Remote Sens-Basel 10(5):690. https://doi.org/10.3390/rs10050690

Oke PR, Pilo GS, Ridgway K, Kiss A, Rykova T (2019) A search for the Tasman front. J Marine Syst 199:103217. https://doi.org/10.1016/j.jmarsys.2019.103217

Pattiaratchi CB, Siji P (2020) Variability in ocean currents around Australia. In: Richardson AJ, Eriksen R, Moltmann T, Wallis JR, Hodgson-Johnston I (eds) State and trends of Australia's ocean report. IMOS, Hobart, p 1.4.1-1.4.6

Pattiaratchi C, Woo M (2009) The mean state of the Leeuwin current system between North West Cape and Cape Leeuwin. J R Soc West Aust 92:221–241

Pearce A, Feng M (2007) Observations of warming on the Western Australian continental shelf. Mar Freshwater Res 58(10):914–920. https://doi.org/10.1071/MF07082

Qiu B, Chen S (2004) Seasonal modulations in the eddy field of the South Pacific ocean. J Phys Oceanogr 34(7):1515–1527. https://doi.org/10.1175/1520-0485(2004)034%3c1515:SMITEF%3e2.0.CO;2

Ridgway KR (2007) Long-term trend and decadal variability of the southward penetration of the East Australian current. Geophys Res Lett 34(13):L13613. https://doi.org/10.1029/2007GL030393

Ridgway KR, Dunn JR (2003) Mesoscale structure of the mean East Australian current system and its relationship with topography. Prog Oceanogr 56(2):189–222. https://doi.org/10.1016/S0079-6611(03)00004-1

Ridgway KR, Godfrey JS (2015) The source of the Leeuwin current seasonality. J Geophys Res-Oceans 120(10):6843–6864. https://doi.org/10.1002/2015JC011049

Roberts JJ, Best BD, Dunn DC, Treml EA, Halpin PN (2010) Marine geospatial ecology tools: an integrated framework for ecological geoprocessing with ArcGIS, Python, R, MATLAB, and C++. Environ Modell Softw 25(10):1197–1207. https://doi.org/10.1016/j.envsoft.2010.03.029

Royer F, Fromentin JM, Gaspar P (2004) Association between bluefin tuna schools and oceanic features in the western Mediterranean. Mar Ecol-Prog Ser 269:249–263. https://doi.org/10.3354/meps269249

Sallée JB, Morrow R, Speer K (2008) Eddy heat diffusion and subantarctic mode Water formation. Geophys Res Lett 35(5):L05607. https://doi.org/10.1029/2007GL032827

Saraceno M, Provost C, Piola AR (2005) On the relationship between satellite-retrieved surface temperature fronts and chlorophyll a in the western South Atlantic. J Geophys Res-Oceans 110(C11):C11016. https://doi.org/10.1029/2004JC002736

Sarkar K, Aparna SG, Dora S, Shankar D (2019) Seasonal variability of sea-surface temperature fronts associated with large marine ecosystems in the north Indian ocean. J Earth Syst Sci 128(1):20. https://doi.org/10.1007/s12040-018-1045-x

Sato M, Barth JA, Benoit-Bird KJ, Pierce SD, Cowles TJ, Brodeur RD, Peterson WT (2018) Coastal upwelling fronts as a boundary for planktivorous fish distributions. Mar Ecol-Prog Ser 595:171–186. https://doi.org/10.3354/meps12553

Snyder S, Franks PJ, Talley LD, Xu Y, Kohin S (2017) Crossing the line: Tunas actively exploit submesoscale fronts to enhance foraging success. Limnol Oceanogr Lett 2(5):187–194. https://doi.org/10.1002/lol2.10049

Stukel MR, Aluwihare LI, Barbeau KA, Chekalyuk AM, Goericke R, Miller AJ, Ohman MD, Ruacho A, Song H, Stephens BM, Landry MR (2017) Mesoscale ocean fronts enhance carbon export due to gravitational sinking and subduction. P Natl A Sci 114(6):1252–1257. https://doi.org/10.1073/pnas.1609435114

Ullman DS, Cornillon PC (1999) Satellite-derived sea surface temperature fronts on the continental shelf off the northeast US coast. J Geophys Res-Oceans 104(C10):23459–23478. https://doi.org/10.1029/1999JC900133

Vázquez DP, Atae-Allah C, Escamilla PLL (1999) Entropic approach to edge detection for SST images. J Atoms Ocean Tech 16(7):970–979. https://doi.org/10.1175/1520-0426(1999)016%3c0970:EATEDF%3e2.0.CO;2

Waite AM, Thompson PA, Pesant S, Feng M, Beckley LE, Domingues CM, Gaughan D, Hanson CE, Holl CM, Koslow T, Meuleners M (2007) The Leeuwin current and its eddies: an introductory overview. Deep-Sea Res Pt II 54(8–10):789–796. https://doi.org/10.1016/j.dsr2.2006.12.008

Wen C, Wang Z, Wang J, Li H, Shi X, Gao W, Huang H (2023) Variation of the coastal upwelling off south java and their impact on local fishery resources. J Ocean Limnol 41:1389–1404. https://doi.org/10.1007/s00343-022-2031-3

Williams RG, Wilson C, Hughes CW (2007) Ocean and atmosphere storm tracks: the role of eddy vorticity forcing. J Phys Oceanogr 37(9):2267–2289. https://doi.org/10.1175/JPO3120.1

Wirasatriya A, Hosoda K, Setiawan JD, Susanto RD (2020) Variability of diurnal sea surface temperature during short term and high SST event in the western equatorial pacific as revealed by satellite data. Remote Sens-Basel 12(19):3230. https://doi.org/10.3390/rs12193230

Wolanski E, Hamner WM (1988) Topographically controlled fronts in the ocean and their biological influence. Science 241(4862):177–181. https://doi.org/10.1126/science.241.4862.177

Woodson CB, Litvin SY (2015) Ocean fronts drive marine fishery production and biogeochemical cycling. P Natl A Sci 112(6):1710–1715. https://doi.org/10.1073/pnas.1417143112

Xu Y, Nieto K, Teo SL, McClatchie S, Holmes J (2017) Influence of fronts on the spatial distribution of albacore tuna (Thunnus alalunga) in the Northeast pacific over the past 30 years (1982–2011). Prog Oceanogr 150:72–78. https://doi.org/10.1016/j.pocean.2015.04.013

Yang K, Meyer A, Strutton PG, Fischer AM (2023) Global trends of fronts and chlorophyll in a warming ocean. Commun Earth Environ 4:489. https://doi.org/10.1038/s43247-023-01160-2

Yue S, Wang C (2004) The Mann-Kendall test modified by effective sample size to detect trend in serially correlated hydrological series. Water Resour Manag 18(3):201–218. https://doi.org/10.1023/B:WARM.0000043140.61082.60

Zilberman NV, Roemmich DH, Gille ST, Gilson J (2018) Estimating the velocity and transport of western boundary current systems: a case study of the east Australian current near Brisbane. J Atoms Ocean Tech 35(6):1313–1329. https://doi.org/10.1175/JTECH-D-17-0153.1

Publisher's Note Springer Nature remains neutral with regard to jurisdictional claims in published maps and institutional affiliations.